Cell Reports, Volume *40*

Supplemental information

Stromal remodeling regulates dendritic cell abundance and activity in the tumor microenvironment

Athanasios Papadas, Gauri Deb, Alexander Cicala, Adam Officer, Chelsea Hope, Adam Pagenkopf, Evan Flietner, Zachary T. Morrow, Philip Emmerich, Joshua Wiesner, Garrett Arauz, Varun Bansal, Karla Esbona, Christian M. Capitini, Kristina A. Matkowskyj, Dustin A. Deming, Katerina Politi, Scott I. Abrams, Olivier Harismendy, and Fotis Asimakopoulos

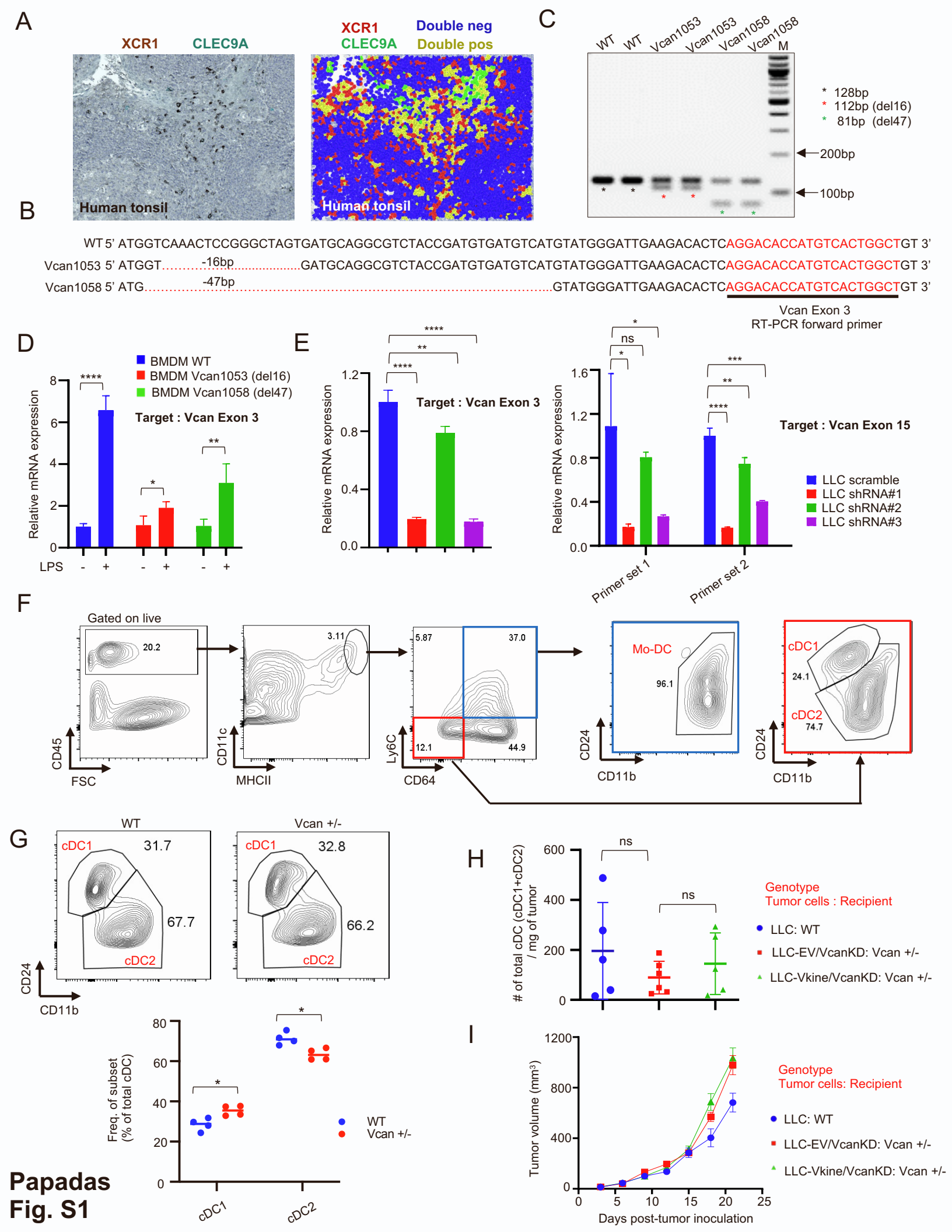

Papadas Fig. S1

Supplementary Fig. S1 (related to Fig. 1). The VCAN pathway regulates tumor cDC1. A: Human tonsil immunohistochemical staining for cDC1 lineage markers XCR1 and CLEC9A. See STAR Methods for protocol. Left, composite image after spectral unmixing. XCR1 (brown, DAB), CLEC9A (teal). Right, scoring map: blue, double-negative; red, single-positive XCR1; green, single-positive CLEC9A; yellow, double-positive XCR1/CLEC9A. 23 different areas were imaged, each containing approximately 4173 cells. About 80% of cells had no expression of markers and ~14% had dual staining. B: Schematic depiction of the deletions in the two mutant *Vcan* founders, 1053 (16bp deletion) and 1058 (47bp deletion). Sequence of exon 3 primer used in RT-PCR experiments shown in red. C: DNA amplification using primers flanking the targeted region. Shown are a 128bp WT amplicon and the mutated amplicons in founders *Vcan*1053 and *Vcan*1058. D: Bone marrow-derived macrophage (BMDM) *Vcan* locus RT-PCR using exon 3 primers at baseline or after stimulation with TLR4 agonist, lipopolysaccharide (LPS). *Vcan*1053 demonstrates a more severe defect in *Vcan* message induction/stability than *Vcan*1058. E: Validation of *Vcan* knockdown in LLC^{VcanKD} cells. LLC cells were transfected with each of 3 hairpins (shRNA #1, 2 or 3) targeting exon 8 (encoding GAGβ domain depicted in red in Fig. 1A). *Vcan* message was assayed using exon 3 primers (left) and exon 15 primers (right). F: Gating strategy to delineate tumor-associated dendritic cells (TADC) per van Ginderachter schema (Laoui et al., 2016). G: cDC subset frequencies in steady-state splenic tissue from WT and *Vcan*-/- mice. H: Total cDC (cDC1 + cDC2) absolute counts per mg tumor mass in LLC: WT, Vcan-depleted (LLC-EV^{VcanKD}: Vcan+/-) and versikine-rescue (LLC-Vkine^{VcanKD}: Vcan+/-) tumors, using the Collagenase/Hyaluronidase tumor cell dissociation protocol (see STAR Methods). I: Growth rates of WT, Vcan-depleted (LLC-EV ^{VcanKD}: Vcan+/-) and versikine-rescue (LLC-Vkine^{VcanKD}: Vcan+/-) tumors. In H and I, the colon separates the genotype of implanted tumor cells from genotype of recipient animal.

Data are presented as mean ± SEM. *p<0.05; **p<0.01; ***p<0.001. *In vitro* experiments were performed in technical triplicates. *In vivo* cohort sizes are shown in individual panels. All experiments were reproduced independently at least twice.

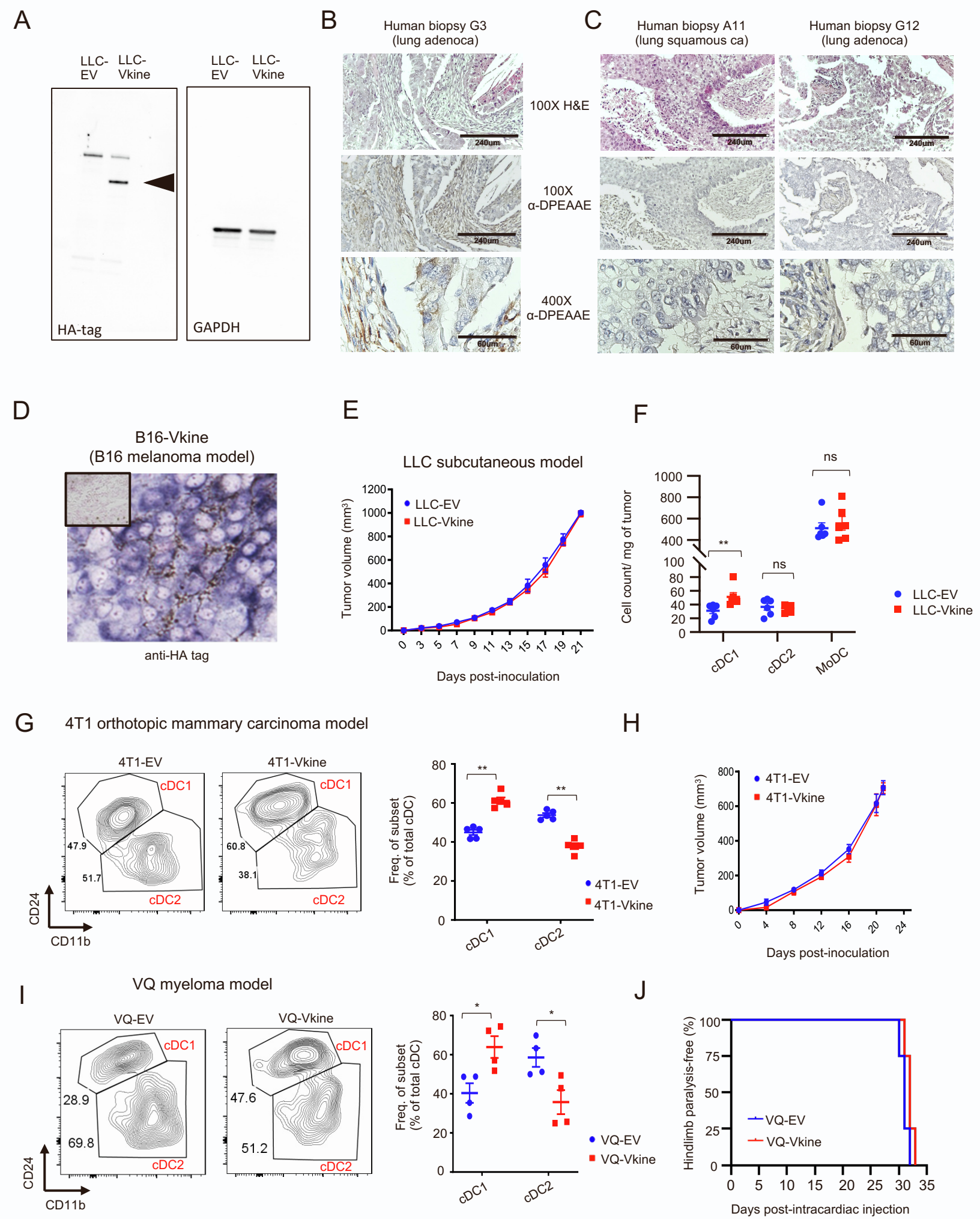

Papadas Fig. S2

Supplementary Fig. S2 (related to Fig. 2). The VCAN-matrikine, versikine, promotes cDC1 abundance *in vivo*. A: Full-length western blot for Fig. 2C. Arrow, versikine band migrating at 75KDa. B: Example of human lung cancer biopsy with stromal plus epithelial DPEAAE staining. 10X objective: scalebar 240mm, 40X objective: scalebar 60mm. C: Examples of negative DPEAAE staining in human lung cancer biopsies. 10X objective: scalebar 240mm, 40X objective: scalebar 60mm. See Supp. Table S1 for summary of staining patterns. D: Membranous localization of HA-tagged ectopic versikine in B16 melanoma, a tumor model characterized by absence of cell-autonomous *Vcan* expression (Asano et al., 2017). HA-tag, chromogen: BCIP/NBT; counterstain: nuclear fast red. E: Growth rates of subcutaneous LLC-EV and LLC-Vkine tumors. F: Absolute counts (cell count/ mg of tumor) of major intratumoral DC subsets, following optimized cell dissociation protocols (Miltenyi Dissociation Kit, see STAR Methods). G: Flow cytometric analysis of cDC subsets in orthotopically-implanted 4T1 mammary carcinoma tumors engineered to express empty-vector (4T1-EV) or versikine (4T1-Vkine). Representative flow plots (left) and frequencies (right) of cDC subsets are shown. H: Growth rates of orthotopic 4T1-EV and 4T1-Vkine tumors. I: Flow cytometric analysis of cDC subsets from bone marrow following intracardiac injection of VQ myeloma cells, engineered to express empty-vector (VQ-EV) or versikine (VQ-Vkine). Representative flow plots (left) and frequencies (right) of cDC subsets are shown. J: Kaplan-Meier curves depicting time-to-hindlimb paralysis (a clinical sequela of myeloma progression) in recipients of VQ-EV vs. VQ-Vkine myeloma tumors.

Data are presented as mean ± SEM. *$p<0.05$; **$p<0.01$; ***$p<0.001$. *In vitro* experiments were performed in technical triplicates. *In vivo* cohort sizes are shown in individual panels. All experiments were reproduced independently at least twice.

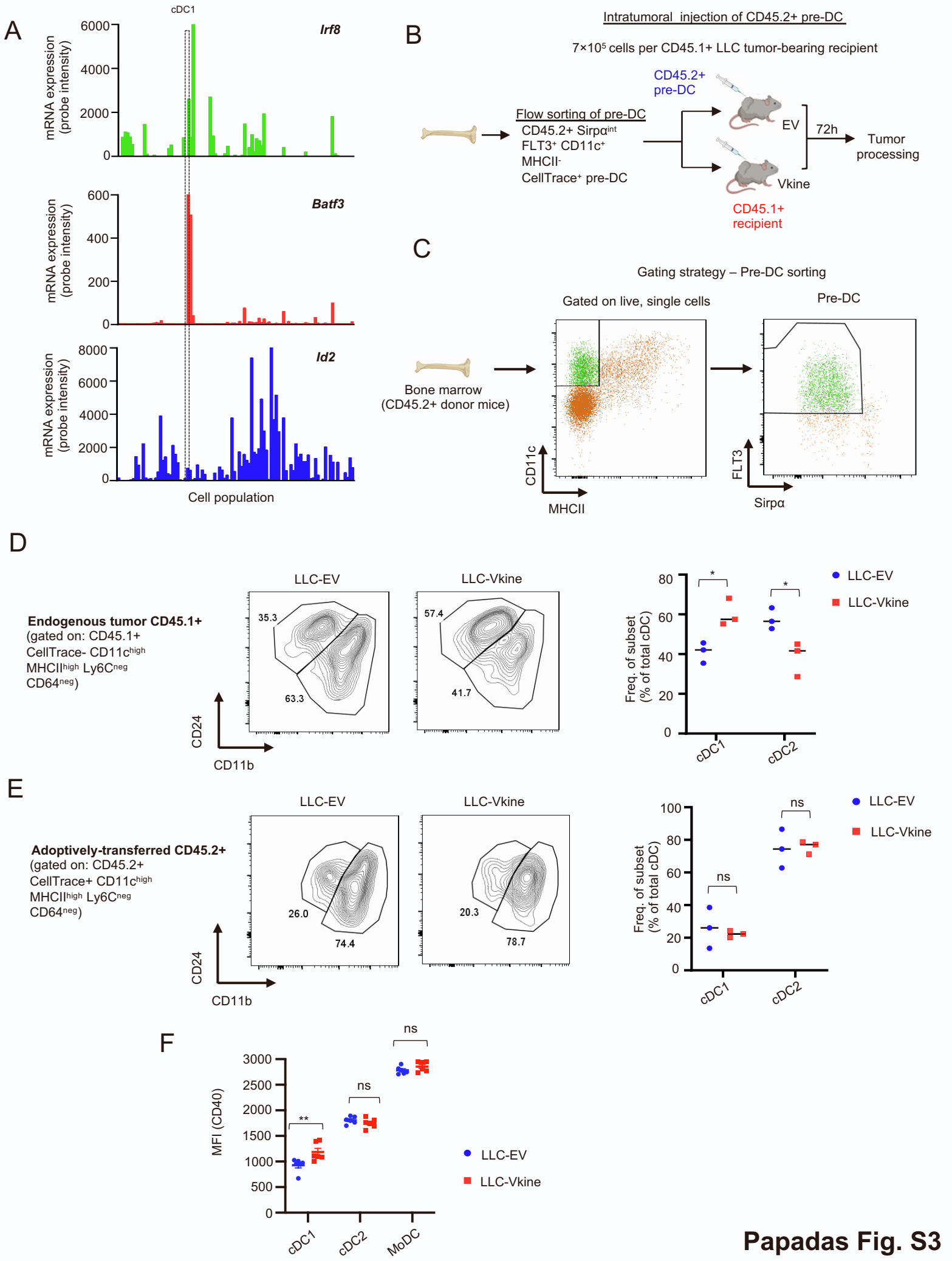

Papadas Fig. S3

Supplementary Fig. S3 (related to Fig. 3). Versikine selectively activates cDC1 *in vivo*. A: Expression pattern of murine *Irf8, Batf3 and Id2*. Data from BioGPS. See Supp. Table S3 for tissue/ lineage annotations. B: Schematic layout of the pre-DC adoptive transfer experiment. Pre-DC were harvested from the BM of Flt3l-*in vivo* mobilized CD45.2+ mice and adoptively transferred into LLC-EV or LLC-Vkine tumors implanted in CD45.1+ recipients. *In vivo* pre-DC mobilization was achieved through implantation of Flt3l-secreting B16 cells, according to standard protocols (Vremec, 2016). 72 hours post-adoptive transfer, tumors were harvested, processed and cDC subsets were analyzed by flow cytometry. C: Gating strategy for flow sorting pre-DC from BM of Flt3l-*in vivo* mobilized donors, per the schema of van Ginderachter (Laoui et al., 2016). D: Representative flow plots of CD45.1+ endogenous cDC subsets (left) and frequencies (right). E: Representative flow plots of CD45.2+ adoptively-transferred cDC subsets (left) and frequencies (right). F: Summary of CD40 staining intensity (MFI= mean fluorescence intensity) in DC subsets from LLC-EV and LLC-Vkine tumors (independent Experiment 2).

Data are presented as mean ± SEM. *p<0.05; **p<0.01; ***p<0.001. *In vitro* experiments were performed in technical triplicates. *In vivo* cohort sizes are shown in individual panels. All experiments were reproduced independently at least twice.

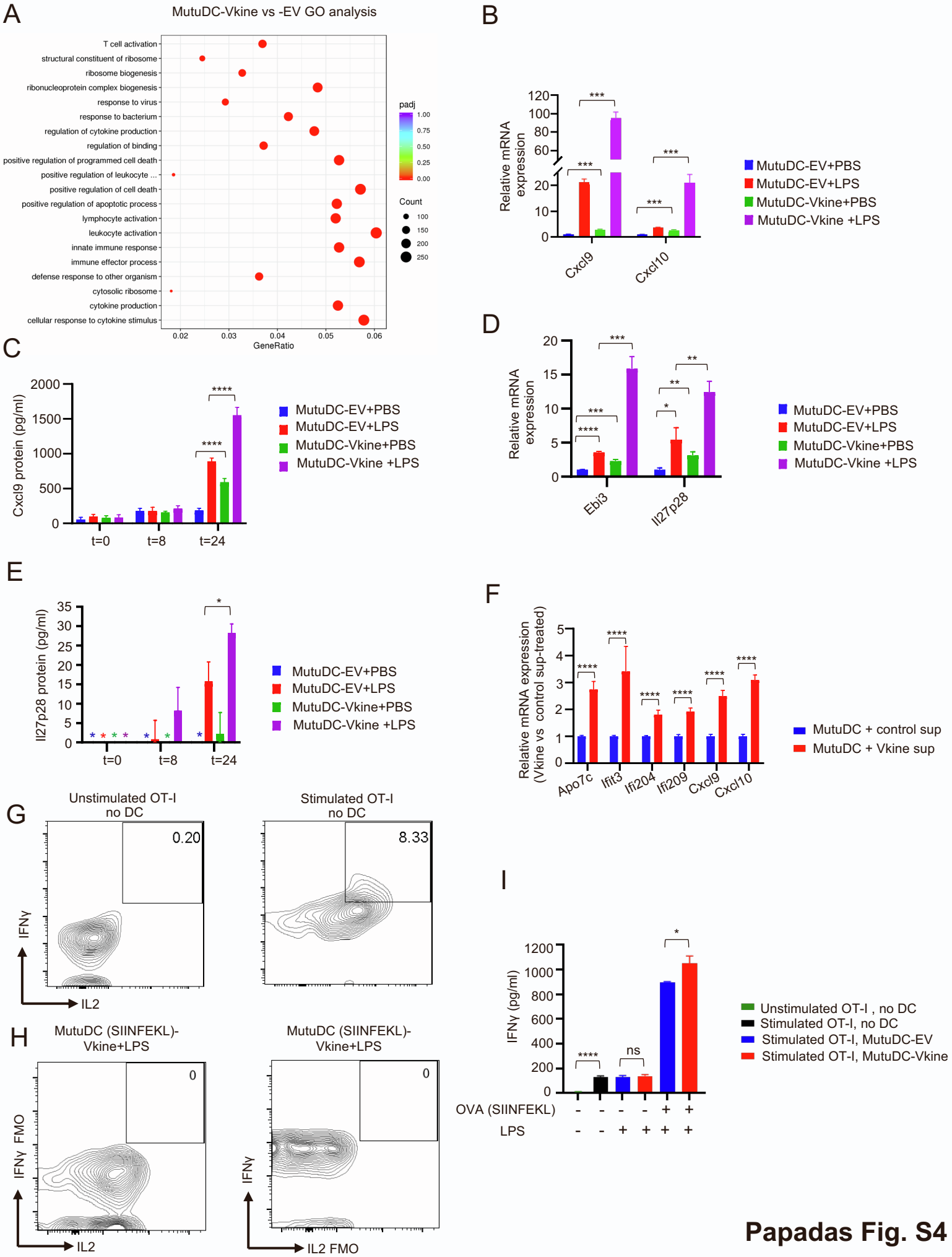

Papadas Fig. S4

Supplementary Fig. S4 (related to Fig. 4). cDC1 activation by versikine is cell-autonomous. A: Gene ontology (GO) pathway analysis of differentially expressed genes between MutuDC1940-Vkine vs. -EV. Versikine's proapoptotic program ("positive regulation of programmed cell death/ "positive regulation of apoptotic process") is reminiscent of versikine's proapoptotic activities during development (McCulloch et al., 2009). B: RT-PCR of Cxcl9/10 in MutuDC1940-EV vs. MutuDC1940-Vkine stimulated with TLR4 agonist LPS or vehicle (PBS). C: ELISA detection of secreted Cxcl9 by MutuDC1940-EV- and MutuDC1940-Vkine stimulated with LPS or vehicle (PBS) plotted against time (hours). D: RT-PCR for Il27p28 and Ebi3 message in MutuDC1940-EV-vs. -Vkine stimulated with LPS or vehicle (PBS). E: ELISA detection of secreted Il27p28 by MutuDC1940-EV- and MutuDC1940-Vkine stimulated with LPS or vehicle (PBS) plotted against time (hours). F: RT-PCR for selected versikine-signature genes using RNA from MutuDC1940 cells (unmanipulated) exposed to supernatant from versikine-secreting HEK293 cells (Vkine sup) vs. control supernatant (control sup) at 72 hours. G: Flow cytometry for endogenous IFNγ and IL2 of OT-I CD8+ T cells at baseline (left) and PMA-stimulated, prior to addition of DC (right). H: FMO controls shown for IFNγ (left) and IL2 (right) under conditions of maximal stimulation (Vkine +LPS, compare to Fig. 4I). I: IFNγ by ELISA in supernatants from OT-I+ MutuDC1940:SIINFEKL co-cultures in the antigen presentation assay.

Data are presented as mean ± SEM. ns, non-significant, *$p<0.05$; **$p<0.01$; ***$p<0.001$; ****$p<0.0001$. *In vitro* experiments were performed in technical triplicates. *In vivo* cohort sizes are shown in individual panels. All experiments were reproduced independently at least twice.

Papadas Fig. S5

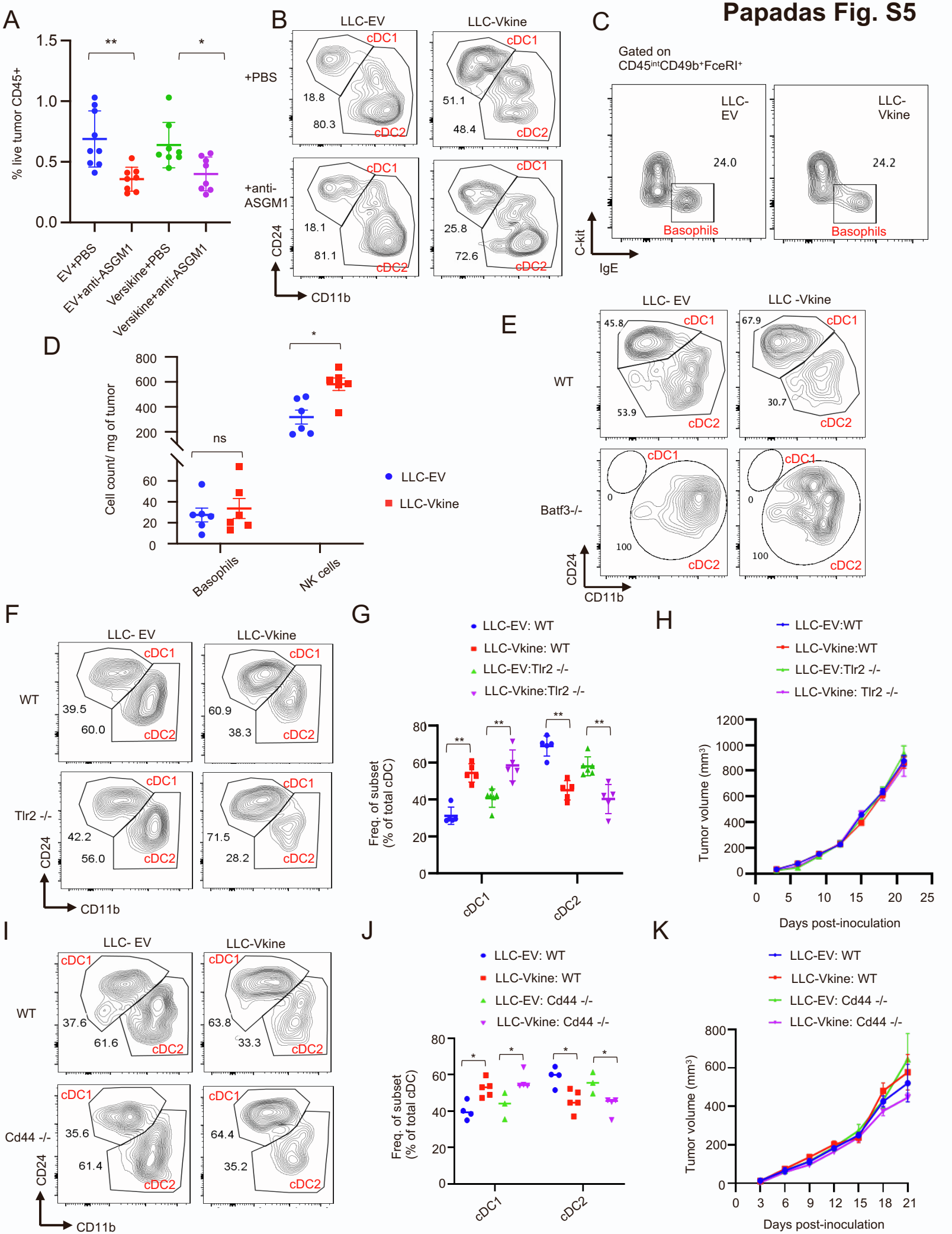

Supplementary Fig. S5 (related to Fig. 5). cDC1 accumulation requires atypical innate lymphoid support. A: Validation of intratumoral NK (NK1.1+CD49b+) depletion following anti-ASGM1 treatment. B: Flow cytometric analysis of cDC subsets in LLC-EV vs. LLC-Vkine tumors following treatment with NK-depleting antibody (anti-ASGM1) or vehicle (PBS). C: Flow cytometric analysis of intratumoral basophils (defined as $CD45^{int}CD49b^{+}Fc\epsilon RI^{+}IgE^{+}c\text{-}Kit^{-}$ cells, gating per (Sektioglu et al., 2017)). D: Absolute counts/ mg tumor tissue of intratumoral basophils compared to intratumoral NK1.1+CD3- cells, in LLC-EV vs. LLC-Vkine tumors. E: Absence of intratumoral cDC1 in *Batf3*-/- recipients by multiparametric flow cytometry. F: Flow cytometric analysis of cDC subsets in LLC-EV vs. LLC-Vkine tumors implanted in WT or *Tlr2*-/- recipients. G: Summary of cDC subset frequency by flow cytometric analysis in LLC-EV vs. LLC-Vkine tumors implanted in WT or *Tlr2*-/- recipients. H: Growth rates of LLC-EV and LLC-Vkine tumors in WT vs. *Tlr2*-/- background. I: Flow cytometric analysis of cDC subsets in LLC-EV vs. LLC-Vkine tumors implanted in WT or *Cd44*-/- recipients. J: Summary of cDC subset frequency by flow cytometric analysis in LLC-EV vs. LLC-Vkine tumors implanted in WT or *Cd44*-/- recipients. K: Growth rates of LLC-EV and LLC-Vkine tumors in WT vs. *Cd44*-/- genetic background.

Data are presented as mean ± SEM. *$p<0.05$; **$p<0.01$; ***$p<0.001$. *In vitro* experiments were performed in technical triplicates. *In vivo* cohort sizes are shown in individual panels. All experiments were reproduced independently at least twice.

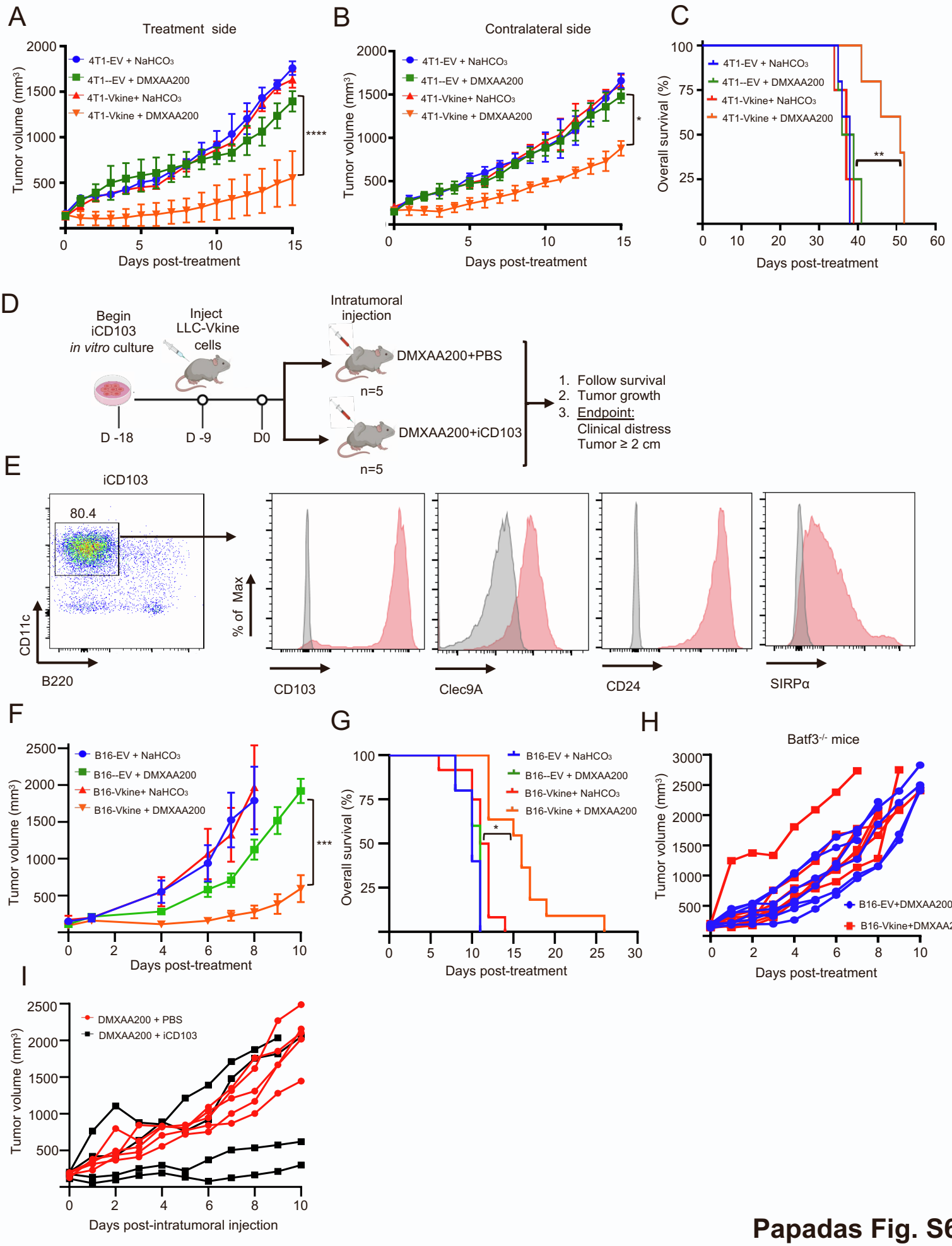

Papadas Fig. S6

Supplementary Fig. S6 (related to Fig. 6). Stroma-licensed cDC1 are "poised" and hypersensitive to nucleic acid sensing *in vivo*. A: Versikine-DMXAA synergy generates an abscopal effect in 4T1 mammary carcinomas. Growth curves of treatment-side 4T1-EV and 4T1-Vkine tumors challenged with a single sub-therapeutic dose (200 mcg) of IT DMXAA on Day 0 (DMXAA200) or vehicle (NaHCO3). B: Growth curves of contralateral side unmanipulated 4T1 tumors, according to corresponding treatment side configuration (treatment as in Panel S6A). C: Versikine-induced abscopal effect is accompanied by a survival advantage in 4T1 tumors. **=$p<0.01$ by log-rank test. D: Schematic layout of iCD103 cell adoptive transfer experiments. E: Flow-cytometric validation of the iCD103 cells, generated as described in the protocol by Merad, Sparwasser and colleagues (Mayer et al., 2014), using standard cDC1 markers. F: Growth curves of B16-EV and B16-Vkine tumors challenged with a single subtherapeutic dose (200 mcg) of IT DMXAA on Day 0 (DMXAA200) or vehicle (NaHCO3). G: Kaplan-Meier survival curves for the experiment in panel S6F, *=$p<0.05$ by log-rank test. H: Response to DMXAA200 is lost in B16-Vkine tumors implanted in *Batf3*-/- recipients. I: Efficacy of sub-therapeutic DMXAA200 in B16-Vkine tumors implanted in *Batf3*-/- recipients is restored following adoptive transfer of iCD103 cells. A subset of B16-bearing tumors did not "take" iCD103 cells, likely attributable to the pauci-immune environment of B16 tumors.

In vitro experiments were performed in technical triplicates. *In vivo* cohort sizes are shown in individual panels. All experiments were reproduced independently at least twice.

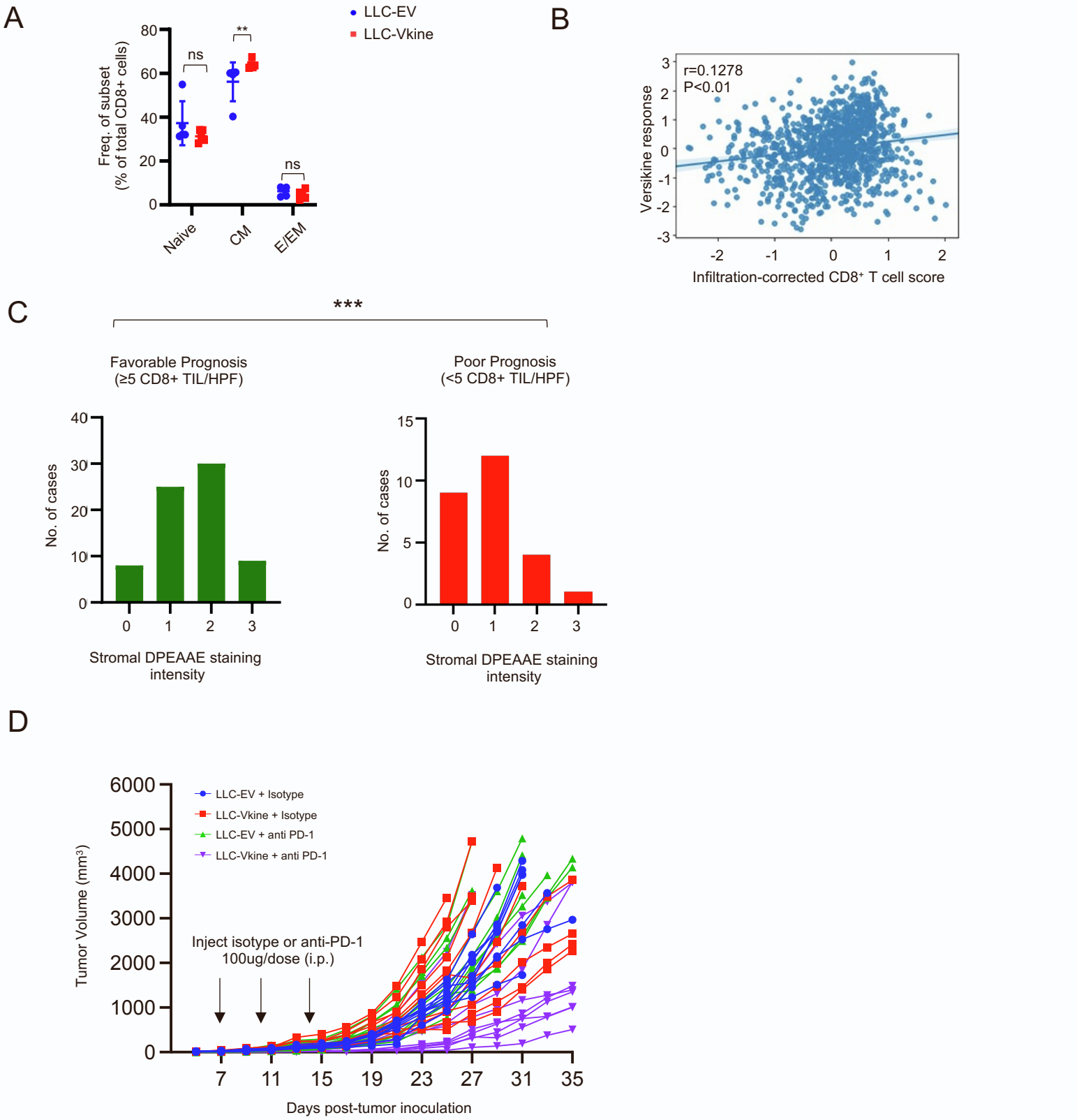

Papadas Fig. S7

Supplementary Fig. S7 (related to Fig. 7). Versikine promotes CD8+ responses and overcomes resistance to anti-PD1 inhibitors *in vivo*. A: CD8+ T cell subset frequency in the spleen of mice treated as in the schema depicted in Fig. 7A. Naïve (CD44-CD62L+), central memory [CM, (CD44+CD62L+)], effector/ effector memory [E/EM, (CD44+CD62L-)]. B: Correlation between *in vitro* versikine response signature and corrected CD8+ T cell scores across TCGA lung cancers. CD8+ T cell scores corrected for immune infiltration to remove variation associated with immune state. C: Distribution of DPEAAE stromal staining intensity across lung cancer prognostic subgroups [pauci-immune (poor prognosis) and immune-rich (favorable prognosis) at cutoff 5 CD8+ TIL/HPF]. Low DPEAAE staining intensities are more prevalent in the pauci-immune subgroup than the immune-rich subgroup, $p<0.001$ by two-tailed Mann-Whitney test. D: Growth response curves of individual tumors in the anti-PD1 experiment depicted in Fig. 7F.

Data are presented as mean ± SEM. *$p<0.05$; **$p<0.01$; ***$p<0.001$. *In vitro* experiments were performed in technical triplicates. *In vivo* cohort sizes are shown in individual panels. All experiments were reproduced independently at least twice.